Asociación Argentina
de Mecánica Computacional

Mecánica Computacional Vol XXIX, págs. 8263-8279 (artículo completo)
Eduardo Dvorkin, Marcela Goldschmit, Mario Storti (Eds.)
Buenos Aires, Argentina, 15-18 Noviembre 2010

STRUCTURAL SHAPE CONTROL USING MACRO FIBER COMPOSITE PIEZOELECTRIC SENSORS AND ACTUATORS

Caio dos Santos Guimarães[a], Flávio Luiz de Silva Bussamra[a], Valérie Pommier-Budinger[b] , José Antônio Hernandes[a]

[a]*Instituto Tecnológico de Aeronáutica - ITA, Praça Marechal Eduardo Gomes, 50, São José dos Campos, SP, Brazil, caioguima@gmail.com, flaviobu@ita.br, Hernandes@ita.br , http://www.ita.br*

[b]*Université de Toulouse – ISAE, 10, avenue Édouard Belin -. BP 54032 - 31055 Cedex 4, Toulouse, France, valerie.budinger@isae.fr , http://www.isae.fr*

Keywords: smart structures, active control, piezoelectric sensors and actuators, piezoelectric macro fiber composites, stability of structures.

Abstract. This article presents an approach for sizing and positioning piezoelectric Macro Fiber Composite (MFC) components for attenuating structural vibration. Even though this new material has become popular in the domain of structural vibration control for its easy conformability and repeatable manufacturing process, as well as their durability and efficiency, little is still known regarding the theoretical modeling of these piezoelectric components and their implementation in Finite Element Method software. Being designed empirically, one could say that MFCs have been poorly investigated when it comes to understanding their actuation properties as a function of their design parameters and electrical properties. The article proposes a finite element method to design smart structures with MFCs. An experimental model of a controlled clamped beam was used to validate the numerical results of the proposed method. The actuation and sensing capabilities of these MFC components are then compared to normal hard piezoelectric ceramics findings.

1 INTRODUCTION

One of the most important topics in the study of Structures in Engineering is stability. The interest in stability can be kindled by many different research areas, one of which is the one to be studied in this work: the shape of structures.

Active Control is needed when undesired shape changing occurs through time. A feedback system is then needed so that the input voltage can be chosen as a function of its instant shape changing. The main idea in active control is to cancel out certain vibration by creating a source of similar vibration in the opposite direction, at each instant. Structures equipped with these control systems are called Smart Structures. They consist basically of a system of actuators and sensors, and a control system.

This technique for vibration control opens up a whole new world of possibilities of specific studies. Research is needed to find the best type of transducers to be used in each case, for example. This study aims on modeling a special type of piezocomposite material using Finite Element Method software ANSYS and comparing its actuation capability results with those of a hard piezoelectric ceramic.

1.1 Piezocomposite Material

The PZT (Lead Zirconate Titanate) is a type of piezoelectric ceramic that has a very good actuation capability. However, difficulty in adapting themselves to complex curved structures as well as their fragile composition limits its use. Piezocomposite transducers are made of an active layer between two electrode layers. The active layer is composed of a mixture of Epoxy Resin and Piezoelectric fibers of materials equivalent to the fore-mentioned piezoelectric ceramics.

One of the main advantages of using composite actuators is the possibility of molding the anisotropic mechanical properties, in order to optimize certain actuating directions. On the other hand, even a very small thin layer of epoxy resin, due to its great difference of dielectric constant in relation to that of the piezoelectric fiber, causes a huge reduction in the electric field to pass by the active layer. So, one of the main concerns in this type of construction is how to dispose the piezoelectric fiber and the epoxy resin matrix between the electrodes.

Between 1997 and 2002, MIT researchers attempted to solve this problem by trying to increase the permittivity of the epoxy resin material, without success. Another proposed solution was to bring the electrodes in direct contact with the fibers, but the manufacturing difficulty made it a process not repeatable (A. DERAEMAEKER, et al., 2007).

An interesting solution appeared with the actuator called Macro Fiber Composites (or simply, MFCs) developed by NASA around the year 2000. The piezoelectric fiber displayed as rectangular piezo-ceramic rods aligned with rectangular layers of the epoxy resin. The advantage lies in the cost of manufacturing (relatively cheap) and its repeatability. The disposition of the fibers allows them to be in direct contact with the electrodes, solving the problem of dielectric mismatch. Two main MFC type patches were developed at the time; the d_{31} type MFC and the d_{33} type (Figure 1). The latter is made to take advantage of the high d_{33} piezoelectric coefficient in order to create higher actuation. Interdigitated electrodes are proposed to maximize the electric field imposition on the direction of the fibers without having to use huge values of voltage.

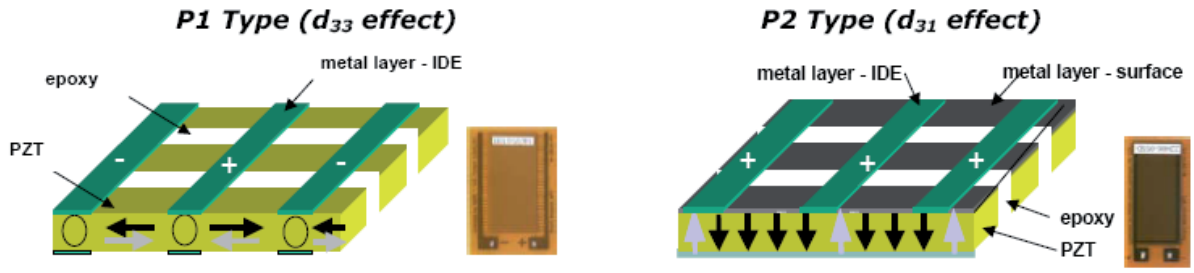

Figure 1 : Piezoelectric MFC (http://www.smart-material.com)

2 MACRO FIBER COMPOSITE (MFC) HOMOGENIZED MODEL

The main component of interest in this study is the d_{31} Macro Fiber Composite actuator that is, as well mentioned by the manufacturer *Smart-Material©,* flexible, durable, and easily conformed to different types of surfaces (see, Smart-Material). The active layer of these piezocomposites has rectangular piezoelectric ceramic fibers, as well as rectangular strips of epoxy resin (Figure 2).

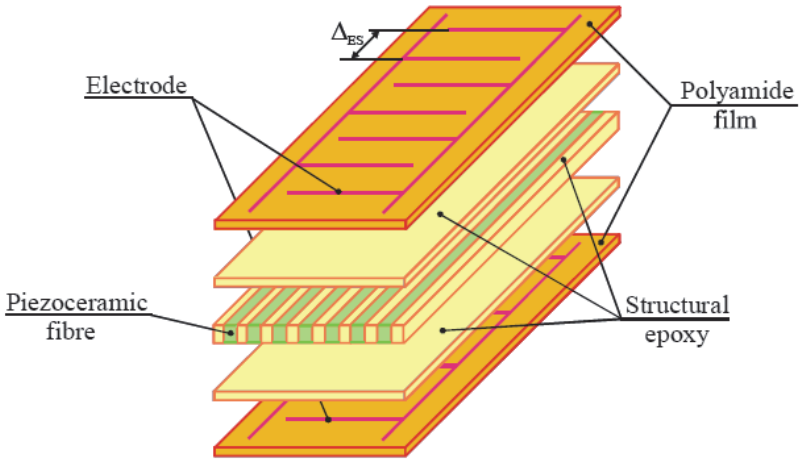

Figure 2 : MFC d_{31} patch components (http://www.smart-material.com)

A simplified representation of this material and its behavior is sought for its Finite Element model. The d_{31} patch can be seen as a 5 layer laminate. The central layer (the active layer) is composed of an Epoxy matrix, and piezoelectric material. According to the manufacturer *Smart Materials*, the volume fraction of fibers in the central layer is approximately 83%, whilst the piezoelectric portion has properties similar to the PZT-5A1 (Table 1). The thickness for each layer is informed by manufacturer as of 0.180 mm for the active layer, 0.03 mm for the epoxy glue and the Kapton film layers, giving a total of 0.3 mm of thickness for the patch. For the piezoelectric components used, the poling direction is perpendicular to its plane.

Piezoceramic Properties	Symbol	unit	Type 5A1
Permittivity	$\varepsilon_{33}^{T}/\varepsilon_0$		1850
Curie Temperature	T_c	^oC	335
Coupling Factors	k_p k_{31} k_{33} k_t k_{15}		0.62 0.33 0.72 0.48 0.74
Piezoelectric charge coefficients	d_{33} $-d_{31}$ d_{15}	10^{-12} C/N	440 185 560
Piezoelectric voltage coefficients	g_{33}	10^{-3} Vm/N	25.5
Compliance	s_{11}^{E} s_{33}^{E}	10^{-12} m²/N	18.5 20.7
Stiffness	c_{33}^{D} c_{55}^{D}	10^{-10} N/m²	15.7 6.5
Poisson's Ratio	υ_{13}		0.38

Table 1 : Properties of Piezoelectric Material 5A1

The equations below describe the standard representation of the Constitutive Equations of the piezoelectric systems, set by the IEEE, 1998. These equations represent the relationship between the dependent mechanical and electrical fields to their independent field variables:

$$\begin{aligned} \{S\} &= s^E.\{T\} + d_t.\{E\}, \\ \{D\} &= d.\{T\} + \varepsilon^T.\{E\}. \end{aligned} \tag{1}$$

where D is the electrical displacement (C/m²), S is the strain vector, E is the electric field vector (V/m), and T is the stress (N/m²), ε^T is the dielectric matrix, d is the induced strain and s^E is the compliance matrix (s^E). The superscript T represents a constant stress condition, while the superscript E represents a constant (if possible, zero) electric field condition. The subscript t indicates the transposed matrix. Equations (1) may also be written in its stiffness form, where the mechanical stress is written as a function of the strain and the electrical field:

$$\begin{aligned} \{T\} &= c^E.\{S\} - e_t.\{E\}, \\ \{D\} &= e.\{S\} + \varepsilon^s.\{E\}. \end{aligned} \tag{2}$$

The material property constants, in this form of writing, are the dielectric matrix (ε^S), the stiffness matrix (c^E), the induced stress matrix (e) and its transposed matrix (e_t), then:

$$\{T\} = \left(s^E\right)^{-1}.\{S\} - \left(s^E\right)^{-1}.d_t.\{E\}. \tag{3}$$

From (1):

$$\{D\} = d\left(s^E\right)^{-1}.\{S\} + \left(\varepsilon^T - d.\left(s^E\right)^{-1}.d_t\right).\{E\}. \tag{4}$$

From which follows the relationship between the property matrices:

$$\begin{cases} \left(s^E\right)^{-1} = c^E \\ e = d.\left(s^E\right)^{-1} = d\ .c^E\ . \\ \varepsilon^S = \varepsilon^T - d.\left(s^E\right)^{-1}.d_t \end{cases} \tag{5}$$

Using the standard IEEE notations, (1) may be re-written as follows, making use of the transverse symmetry of our piezoelectric component:

$$\begin{Bmatrix} T_1 \\ T_2 \\ T_3 \\ T_4 \\ T_5 \\ T_6 \\ D_1 \\ D_2 \\ D_3 \end{Bmatrix} = \begin{bmatrix} c_{11}^E & c_{12}^E & c_{13}^E & 0 & 0 & 0 & 0 & 0 & -e_{31} \\ c_{12}^E & c_{22}^E & c_{23}^E & 0 & 0 & 0 & 0 & 0 & -e_{32} \\ c_{13}^E & c_{23}^E & c_{33}^E & 0 & 0 & 0 & 0 & 0 & -e_{33} \\ 0 & 0 & 0 & c_{44}^E & 0 & 0 & 0 & -e_{24} & 0 \\ 0 & 0 & 0 & 0 & c_{55}^E & 0 & -e_{15} & 0 & 0 \\ 0 & 0 & 0 & 0 & 0 & c_{66}^E & 0 & 0 & 0 \\ 0 & 0 & 0 & 0 & e_{15} & 0 & \varepsilon_{11}^S & 0 & 0 \\ 0 & 0 & 0 & e_{24} & 0 & 0 & 0 & \varepsilon_{22}^S & 0 \\ e_{31} & e_{32} & e_{33} & 0 & 0 & 0 & 0 & 0 & \varepsilon_{33}^S \end{bmatrix} . \begin{Bmatrix} S_1 \\ S_2 \\ S_3 \\ S_4 \\ S_5 \\ S_6 \\ E_1 \\ E_2 \\ E_3 \end{Bmatrix}. \tag{6}$$

The following equations were also taken from A. DERAEMAEKER, et al., 2007, in order to be able to reconstruct the full set of material parameters of the anisotropic mechanical matrix for the piezoelectric material portion:

$$s_{55}^E = \frac{1}{C_{55}^D.\left(1 - k_{55}^2\right)} \tag{7}$$

$$s_{12}^E = -s_{11}^E + 2.\frac{d_{31}^2}{\varepsilon_{33}^T.k_p^2} \tag{8}$$

$$\varepsilon_{11}^T = \frac{d_{15}^2}{s_{55}^E.k_{15}^2} \tag{9}$$

$$s_{13}^E = -\upsilon_{13}.s_{11}^E \tag{10}$$

Also, with the isotropic transverse symmetry assumption:

$$\begin{aligned} &s_{22}^E = s_{11}^E\ ,\ s_{23}^E = s_{13}^E\ , \\ &s_{44}^E = s_{55}^E\ ,\ s_{66}^E = 2.\left(s_{11}^E - s_{12}^E\right), \\ &d_{31} = d_{32}\ ,\ \ d_{24} = d_{15}\ , \\ &\varepsilon_{22}^T = \varepsilon_{11}^T. \end{aligned} \tag{11}$$

The passive layers are considered isotropic materials. Typical values were used for both the Kapton film and the epoxy material. As relative permittivity for the epoxy resin, the typical value of 4.25 was used, and:

$$E_{epoxy} = 2.0\ GPa \qquad \nu_{epoxy} = 0.3 \qquad \rho_{epoxy} = 1100\ {}^{kg}/_{m^3}$$
$$E_{Kapton} = 2.8\ GPa \qquad \nu_{Kapton} = 0.3 \qquad \rho_{Kapton} = 1580\ {}^{kg}/_{m^3}$$

The compliance matrix for the isotropic materials can be expressed by:

$$s^E = \frac{1}{E}\begin{bmatrix} 1 & -\nu & -\nu & 0 & 0 & 0 \\ -\nu & 1 & -\nu & 0 & 0 & 0 \\ -\nu & -\nu & 1 & 0 & 0 & 0 \\ 0 & 0 & 0 & 2.(1+\nu) & 0 & 0 \\ 0 & 0 & 0 & 0 & 2.(1+\nu) & 0 \\ 0 & 0 & 0 & 0 & 0 & 2.(1+\nu) \end{bmatrix}. \tag{12}$$

The MFC datasheet supplied by the manufacturer (SMART-MATERIAL©) does not, however, supply enough information to simulate the d_{31} patch. Information such as the d_{32} coefficient and the shear modulus are not described for all directions, even though it is needed as an input for the simulation. According to A. DERAEMAEKER, et al., 2007, a sensitivity analysis shows that the d_{32} coefficient, not given by the fabricant, can influence significantly depending on the results sought, and should be well estimated.

To model the d_{31}-type MFCs, a mixing rule theory was applied, where mean values of the patch's properties can be calculated to be used as inputs for the finite element software ANSYS.

The approach bases itself on the Uniform Field Method (UFM). The object of the mixing-rule is to find the equivalent property matrix for a material of two constituents. For this, it is assumed that the constitutive equations above can be written in the same way for each of the two constituents. Let us consider a representative volume element (RVE), of the d_{31} patch. Representing the epoxy matrix portion of the material by the superscript m, and the piezoelectric portion by the superscript p, and the volume fraction of piezoelectric material by ρ, the values of T, S, D, E can be represented by their average values:

$$\begin{aligned} \overline{T}_{k=1,\dots,6} &= \rho.T_k^{\,p} + (1-\rho).T_k^{\,m} = \int_V T_k.dV\,, \\ \overline{S}_{k=1,\dots,6} &= \rho.S_k^{\,p} + (1-\rho).S_k^{\,m} = \int_V S_k.dV\,, \\ \overline{D}_{i=1,\dots,3} &= \rho.D_i^{\,p} + (1-\rho).D_i^{\,m} = \int_V D_i.dV\,, \\ \overline{E}_{i=1,\dots,3} &= \rho.E_i^{\,p} + (1-\rho).E_i^{\,m} = \int_V E_i.dV\,. \end{aligned} \tag{13}$$

The Uniform Field Method bases itself on the deformation mechanism for the RVE for each type of deformation. In the case of the d_{31} MFC:

$$\begin{aligned} &\overline{T}_2 = T_2^{\,p} = T_2^{\,m}\ ;\ \overline{T}_4 = T_4^{\,p} = T_4^{\,m}\ ;\ \overline{T}_6 = T_6^{\,p} = T_6^{\,m}\,, \\ &\overline{S}_1 = S_1^{\,p} = S_1^{\,m}\ ;\ \overline{S}_3 = S_3^{\,p} = S_3^{\,m}\ ;\ \overline{S}_5 = S_5^{\,p} = S_5^{\,m}\,, \\ &\overline{E}_1 = E_1^{\,p} = E_1^{\,m}\ ;\ \overline{E}_2 = E_2^{\,p} = E_2^{\,m}\,, \\ &\overline{D}_2 = D_2^{\,p} = D_2^{\,m}\,. \end{aligned} \tag{14}$$

The other parameters will follow the average rule cited in equation (13). If the above expressions are introduced into the constitutive equation (6), then c^E, e, ε as we as $c^{E\ p}$, e^p, ε^p and $c^{E\,m}$, e^m, ε^m become related as follows:

$$\begin{Bmatrix} \overline{T}_1 \\ \overline{T}_2 \\ \overline{T}_3 \\ \overline{T}_4 \\ T_5 \\ \overline{T}_6 \\ \overline{D}_1 \\ \overline{D}_2 \\ \overline{D}_3 \end{Bmatrix} = \begin{bmatrix} c_{11}^E & c_{12}^E & c_{13}^E & 0 & 0 & 0 & 0 & 0 & -e_{31} \\ c_{12}^E & c_{22}^E & c_{23}^E & 0 & 0 & 0 & 0 & 0 & -e_{32} \\ c_{13}^E & c_{23}^E & c_{33}^E & 0 & 0 & 0 & 0 & 0 & -e_{33} \\ 0 & 0 & 0 & c_{44}^E & 0 & 0 & 0 & -e_{24} & 0 \\ 0 & 0 & 0 & 0 & c_{55}^E & 0 & -e_{15} & 0 & 0 \\ 0 & 0 & 0 & 0 & 0 & c_{66}^E & 0 & 0 & 0 \\ 0 & 0 & 0 & 0 & e_{15} & 0 & \varepsilon_{11}^S & 0 & 0 \\ 0 & 0 & 0 & e_{24} & 0 & 0 & 0 & \varepsilon_{22}^S & 0 \\ e_{31} & e_{32} & e_{33} & 0 & 0 & 0 & 0 & 0 & \varepsilon_{33}^S \end{bmatrix} . \begin{Bmatrix} \overline{S}_1 \\ \overline{S}_2 \\ \overline{S}_3 \\ \overline{S}_4 \\ \overline{S}_5 \\ \overline{S}_6 \\ \overline{E}_1 \\ \overline{E}_2 \\ \overline{E}_3 \end{Bmatrix}. \tag{15}$$

$$c_{22}^E = \frac{c_{22}^{E\,p}.c_{22}^{E\,m}}{\rho.c_{22}^{Em} + (1-\rho).c_{22}^{Ep}} \tag{16}$$

$$c_{23}^E = c_{22}^E.\left[\rho.\frac{c_{23}^{E\,p}}{c_{22}^{E\,p}} + (1-\rho).\frac{c_{23}^{E\,m}}{c_{22}^{E\,m}}\right] \tag{17}$$

$$c_{21}^E = c_{22}^E.\left[\rho.\frac{c_{21}^{E\,p}}{c_{22}^{E\,p}} + (1-\rho).\frac{c_{21}^{E\,m}}{c_{22}^{E\,m}}\right] \tag{18}$$

$$c_{33}^E = \rho.c_{33}^{E\,p} + (1-\rho).c_{33}^{E\,m} + \frac{\left(c_{23}^E\right)^2}{c_{22}^E} - \rho.\frac{\left(c_{23}^{Ep}\right)^2}{c_{22}^{Ep}} - (1-\rho).\frac{\left(c_{23}^{Em}\right)^2}{c_{22}^{Em}} \tag{19}$$

$$c_{13}^E = \rho.c_{13}^{E\,p} + (1-\rho).c_{13}^{E\,m} + \frac{c_{23}^E.c_{21}^E}{c_{22}^E} - \rho.\frac{c_{23}^{E\,p}.c_{21}^{E\,p}}{c_{22}^{Ep}} - (1-\rho).\frac{c_{23}^{E\,m}.c_{21}^{E\,m}}{c_{22}^{Em}} \tag{20}$$

$$c_{11}^E = \rho.c_{11}^{E\,p} + (1-\rho).c_{11}^{E\,m} + \frac{\left(c_{21}^E\right)^2}{c_{22}^E} - \rho.\frac{\left(c_{21}^{Ep}\right)^2}{c_{22}^{Ep}} - (1-\rho).\frac{\left(c_{21}^{Em}\right)^2}{c_{22}^{Em}} \tag{21}$$

$$c_{55}^E = \rho.c_{55}^{E\,p} + (1-\rho).c_{55}^{E\,m} \tag{22}$$

$$c_{66}^E = \frac{c_{66}^{E\,p}.c_{66}^{E\,m}}{\rho.c_{66}^{Em} + (1-\rho).c_{66}^{Ep}} \tag{23}$$

$$e_{32} = c_{22}^E.\left[\rho.\frac{e_{32}^p}{c_{22}^{E\,p}} + (1-\rho).\frac{e_{32}^m}{c_{22}^{E\,m}}\right] \tag{24}$$

$$e_{33} = \rho.e_{33}^p + (1-\rho).e_{33}^m + \frac{c_{23}^E.e_{32}}{c_{22}^E} - \rho.\frac{c_{23}^{Ep}.e_{32}^p}{c_{22}^{Ep}} - (1-\rho).\frac{c_{23}^{Em}.e_{32}^m}{c_{22}^{Em}} \tag{25}$$

$$e_{31} = \rho.e_{31}^{p} + (1-\rho).e_{31}^{m} + \frac{c_{21}^{E}.e_{32}}{c_{22}^{E}} - \rho.\frac{c_{21}^{Ep}.e_{32}^{p}}{c_{22}^{Ep}} - (1-\rho).\frac{c_{21}^{Em}.e_{32}^{m}}{c_{22}^{Em}} \tag{26}$$

$$c_{44}^{E} = \frac{A}{B^2 + AC} \tag{27}$$

$$e_{24} = \frac{B}{B^2 + AC} \tag{28}$$

$$\varepsilon_{22}^{S} = \frac{C}{B^2 + AC} \tag{29}$$

$$e_{15} = \rho.e_{15}^{p} + (1-\rho).e_{15}^{m} \tag{30}$$

$$\varepsilon_{11}^{S} = \rho.\varepsilon_{11}^{Sp} + (1-\rho).\varepsilon_{11}^{Sm} \tag{31}$$

$$\varepsilon_{33}^{S} = \rho.\varepsilon_{33}^{Sp} + (1-\rho).\varepsilon_{33}^{Sm} - \frac{e_{32}^{2}}{c_{22}^{E}} + \rho.\frac{e_{32}^{p\,2}}{c_{22}^{Ep}} + (1-\rho).\frac{e_{32}^{m\,2}}{c_{22}^{Em}} \tag{32}$$

$$\rho_{dens} = (\rho).\rho_{dens,p} + (1-\rho).\rho_{dens,m} \tag{33}$$

where:

$$A = \rho.\frac{c_{44}^{Ep}}{e_{24}^{p\,2} + c_{44}^{Ep}.\varepsilon_{22}^{Sp}} + (1-\rho).\frac{c_{44}^{Em}}{e_{24}^{m\,2} + c_{44}^{Em}.\varepsilon_{22}^{Sm}} \tag{34}$$

$$B = \rho.\frac{e_{24}^{p}}{e_{24}^{p\,2} + c_{44}^{Ep}.\varepsilon_{22}^{Sp}} + (1-\rho).\frac{e_{24}^{m}}{e_{24}^{m\,2} + c_{44}^{Em}.\varepsilon_{22}^{Sm}} \tag{35}$$

$$C = \rho.\frac{\varepsilon_{22}^{Sp}}{e_{24}^{p\,2} + c_{44}^{Ep}.\varepsilon_{22}^{Sp}} + (1-\rho).\frac{\varepsilon_{22}^{Sm}}{e_{24}^{m\,2} + c_{44}^{Em}.\varepsilon_{22}^{Sm}} \tag{36}$$

By applying the characteristic values of the epoxy and piezoelectric portions of the central layer to the equations above the characteristic coefficients for an effective homogenized central layer can be calculated. This can be better expressed by the use of the following engineering constants:

$$E_L = \frac{1}{s_{11}^{E}} \qquad E_T = \frac{1}{s_{22}^{E}} \qquad \nu_{LT} = -\frac{s_{21}^{E}}{s_{11}^{E}} \qquad G_{LT} = \frac{1}{s_{66}^{E}}\,. \tag{37}$$

The results are shown in Table 2, where E_L is the Young Modulus in direction of the fiber, E_T is the Young Modulus in the transversal direction, υ_{LT} is the in-plane Poisson Ratio and G_{LT} is the in plane shear modulus.

	Symbol	Value
Young Modulus (GPa)	E_1	45,21
	E_2	12,39
	E_3	40,44
Shear Modulus(GPa)	G_{12}	6,03
	G_{23}	6,68
	G_{31}	17,01
Poisson's Ratio	υ_{12}	0,39
	υ_{23}	0,17
	υ_{13}	0,44
Piezoelectric Constants (C/m²)	e_{31}	-2,227
	e_{32}	-0,671
	e_{33}	16,665
	e_{24}	0,0258
	e_{15}	13,668
Dieletric Relative Constants	$\varepsilon_{11}^T/\varepsilon_0$	1574,8
	$\varepsilon_{22}^T/\varepsilon_0$	24,7
	$\varepsilon_{33}^T/\varepsilon_0$	1528,7
Density (kg/m³) *	$\rho_{density}$	4700

* - Measured in Laboratory

Table 2 : Estimated Mechanical Properties of the MFC

3 METHOD OF VALIDATION

To validate the homogenized model a simple structure of a clamped aluminum beam is tested with 1 piezoelectric actuator, as shown in Figure 3 and Table 3. The results of the finite element simulation, using ANSYS and the experimental results will then be compared regarding the tip transverse displacements.

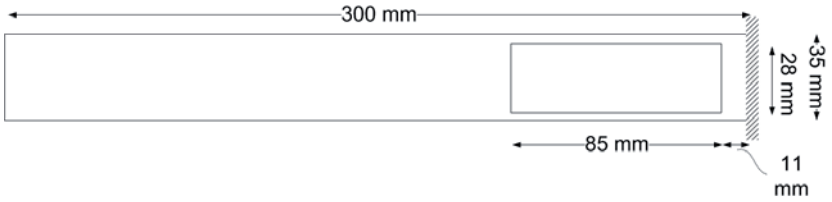

Figure 3 : Experimental setup

	Beam (Aluminum)	Patch
Length (mm)	300	85
Width (mm)	35	28
Thickness (mm)	0.37	0.3
Density (kg/m^3) *	2970	-
Young Modulus (GPa) *	75	-

* - Determined from the mixing rule and have different values for each layer of the patch.

Table 3 : Experimental data

3.1 Finite Element Simulation using ANSYS

The MFC d_{31} modeled patch consists of a layer with the homogenized properties. Seeing as though the size of the patch should have an influence on the final proper frequency values, an adhesive layer was also considered. This thin layer was modeled to be 0.2 mm thick with a 0.5 GPa Young Modulus, and density of 3000 kg/m³. A close-up on this model is given in Figure 4.

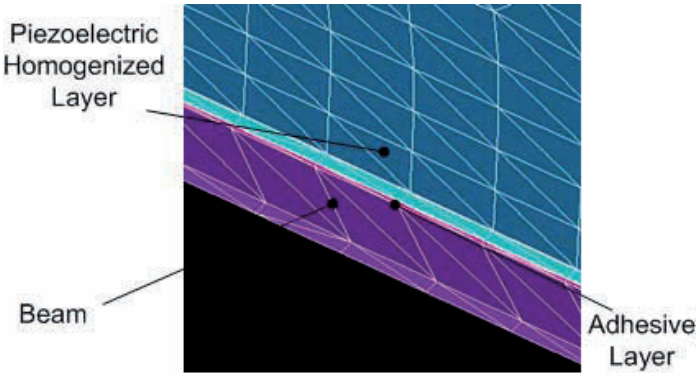

Figure 4 : Patch model layers

The isotropic beam and adhesive layers were modeled with solid tetrahedral elements with 10 nodes (SOLID92). The active layer is modeled with the solid tetrahedral elements with 10 nodes (SOLID98) which includes the displacement as well as the piezoelectric degrees of freedom. Due to incompatibility of attachment between SHELL and SOLID elements, the aluminum beam had to be meshed in solid elements as well.

The electrodes of the patch were set to potential null (short-circuited) as required as boundary condition by setting the surfaces of the central layer to zero voltage. For the first two modes of vibration, the charge on one of the electrodes was calculated using ANSYS, as shown in Table 4.

	Mode 1	Mode 2
Frequency (Hz)	4.795	21.971
Charge	1.094e-3	2.007e-3

Table 4 : Calculated properties for the 'Beam + Patch' simulation

3.2 Theoretical Method of Calculation of the Tip Transverse Displacements

To put the problem into equations, the Lagrange method is used, generalized to include the piezoelectric parameters. The kinetic and potential energy of the piezoelectric system can be initially written as follows:

$$T = \frac{1}{2}\int \rho.u^2.d\Omega\,,$$
$$V = \frac{1}{2}\int T_{ij}.S_{ij}.d\Omega - \frac{1}{2}\int E_i.D_i.d\Omega - v.q_c\,, \tag{38}$$

where Tij and Sij are, respectively, stress and strain tensors of the system. For an active structure with piezoelectric actuators with a supplied voltage of v and electrical charge q_c, electromechanical coupling forces arise, counting for the last term in the expression for the

potential energy. E and D are, respectively, the electric field and the electric displacement field of the system. The full Lagrangian expression, including the electromechanical coupling influence is:

$$L = \frac{1}{2}\int \left(\rho.u^2 - T_{ij}.S_{ij} + E_i.D_i\right).d\Omega. \tag{39}$$

The resulting matrix equations are:

$$\begin{cases} M.\ddot{q} + D_S.\dot{q} + K.q = N.v \\ q_c = N^T.q + C_0.v \end{cases} \tag{40}$$

where M, D, and K are n x n matrices and N is a n x k matrix; q is a vector with the degree of freedom displacements for each element of the geometry. A modeled estimation of the damping factor was included.

$$D_S = \frac{1}{Q_m}.\sqrt{K.M} \tag{41}$$

The quality factor Q_m is a dimensionless parameter that compares the physical system's amplitude to its period, say:

$$Q_m = \frac{f_0}{f_2 - f_1} \tag{42}$$

The parameter f_0 is the resonant frequency and $f_2 - f_1 = \Delta f$, is the width of the range of frequencies for which the energy is at least half of the peak value.

ANSYS can be set to automatically normalize results to the M matrix, i.e. to M-orthonormalize the results. This means that the displacements given by the software form the eigenvectors of the system for each element (generalized coordinate) of the geometry. The dynamic equations of the system can be therefore rewritten as:

$$\begin{cases} M^*.\ddot{u} + D^*.\dot{u} + K^*.u = N^*.v \\ q_c = N^{*T}.u + C_0.v \quad , \quad N^* = \widehat{\Phi}^t.N \end{cases} \tag{43}$$

This transformation makes the mass and stiffness matrices, M* and K*, diagonal (where the first of the two is the identity matrix and the latter a diagonal matrix containing the free vibration frequencies). The characteristic equations in (43) can be expressed in the form of a state-space model:

$$\begin{aligned} \dot{X} &= A.X + B.v \\ Y &= C.X + D.v \end{aligned} \tag{44}$$

where X is the state variable vector constituted of the n displacements and their derivatives in the modal base; v is the input vector of the system; Y is the output vector of the m displacements to be observed in the physical base. From (43) and (44), we can write out the space-state matrices:

$$A = \begin{pmatrix} 0_{nxn} & I_{nxn} \\ -[M^*]^{-1}.[K^*] & -[M^*]^{-1}.[D_s^*] \end{pmatrix} \tag{45}$$

$$B = \begin{pmatrix} 0_{nxk} \\ [M^*]^{-1}.\{N^*\} \end{pmatrix} \tag{46}$$

$$C = \begin{bmatrix} \Phi_m & 0_{m.n} \end{bmatrix} \tag{47}$$

$$D = 0 \tag{48}$$

With the space state in hands, it is possible to compute the Bode diagram for a given voltage supply. The Bode diagram in magnitude will help calculate the theoretical values of the deflection of the structure in a given point. For the resonance frequencies:

$$M.\ddot{x} + K.x + D_s.\dot{x} = N.v\ . \tag{49}$$

From which:

$$\dot{x} = \omega.x = \frac{N.v}{D_s}\ . \tag{50}$$

Therefore, an expression for the deflection at a given point of the structure:

$$x = \frac{N}{\omega D_s}.v = M_{\max}.v\ , \tag{51}$$

where M_{max} is the resonance peak magnitude that can be easily found by observing the Bode Diagram of the system.

3.3 Experimental Setup

In the experimental configuration, a laser vibrometer is used to measure the vibration velocity at a certain point of the structure. A signal generator, a tension amplifier, an electric generator, a charge amplifier, an oscilloscope and a laser vibrometer make up the experimental setup for the verification (Figure 5).

Multiplying the output voltage by the vibration velocity/voltage scale used in the equipment, we have the mean vibration velocity as an output. Knowing how the vibration speed relates to the amplitude q of the movement, the value of q is therefore obtained experimentally by:

$$\Delta v = \omega.\Delta q = 2.\pi.f.\Delta x \tag{52}$$

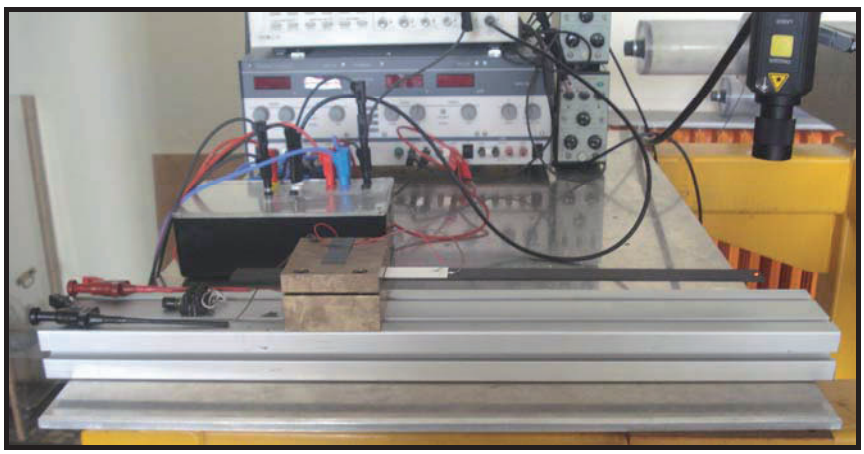

Figure 5 : Experimental setup

3.4 Results Comparison

Results found by V. POMMIER-BUDINGER, et al., 2008 show that the Quality Factor depends strongly on the value of the supply voltage, and this dependence is, in general, non-linear. For this reason, it is absolutely necessary that the voltage used in the calculation of the displacement be the same as the one used for the calculation of the Quality Factor. To calculate the Quality Factor, an input voltage of 8 V was established. The amplitude response output voltage was then measured with the help of an oscilloscope for the first 2 modes of vibration.

Using the system of equations (44), the Bode diagram was traced, as shown in Figure 6. The peak gain magnitudes allow us to find the theoretical displacement values and compare to those measured. The final comparison of the results is shown in Table 5.

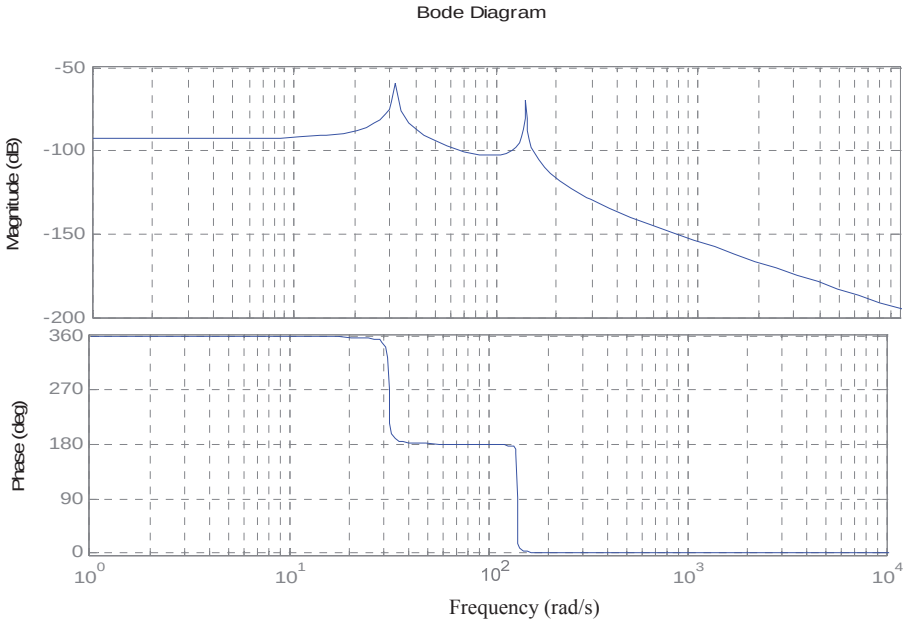

Figure 6 : Bode Diagram of the System

Measurements for supply of 8 V		
Mode	1	2
Measured Frequency (Hz)	4.47	23.43
ANSYS Modeled Frequency (Hz)	4.80	21,97
Quality Factor	40.65	155.6
Output Voltage (V)	1.74	1.82
Experimental Displacement (mm)	7.7	1.6
Theoretical Displacement (mm)	7.7	2.2
Error in Displacement	0.86 %	37,5 %
Error in Proper Frequency	7.36%	- 6,22 %

Table 5 : Proper bending mode frequencies for the clamped beam

4 SIZING AND POSITIONING METHOD

Sizing an active control system consists of determining the volume and position of piezoelectric patch that will give N.v = - F, where F is the external perturbation that should be cancelled. Knowing precisely how many patches to use can mean saving money (by not using more piezoelectric patches than needed), and can also mean protecting the structure (by not using less piezoelectric patches than needed). The existence of a maximum value of the electric field that can be applied to the piezoelectric patch, and a maximum stress that can be supported gives the idea of the maximum value of vibratory amplitude that it can generate by:

$$q_{\max,electric} = \frac{N.v}{\omega.D} = \frac{N.E_{\max}.h}{\omega.D}\,, \tag{53}$$

where E_{max} is the maximum electric field that can be applied, and h is the thickness of the patch. Alternatively, the maximum amplitude can be calculated by:

$$q_{\max,rupture} = \frac{T_{\max}}{T_m / q}, \tag{54}$$

Where T_{max} is the maximum tensile stress supported by the patch, given by the manufacturer. The ratio Tm/q is the ratio maximum stress/deformation, given by ANSYS as an output. In order to account for the uncertainties of the model, the maximum value of vibratory oscillation generated by the piezoelectric patch is estimated to be:

$$q_{\max} = 0.8 \min\left(q_{\max,electric}\ ,\ q_{\max,rupture}\right) \tag{55}$$

5 MFC AND HARD CERAMICS COMPARISON

The piezoelectric components being reasonably modeled, and calculated to give good predictions to the first mode of bending, a comparison of the actuating capability of each of them was made. Naturally, the available patches have different sizes. Seeing as the hard PZT ceramic can be easily cut without altering its configuration, the FEM predictions were tested for a same transversal area as that of the MFC patch (85 mm x 28 mm).

The PZT ceramics available by the fabricant and that are closest to the MFC patch thickness (0.3 mm) are 0.5 mm thick. The piezoelectric constants for the ceramics are given by the manufacturer. For this FEM analysis, the same adhesive layer was used in both cases, with the same properties as the one already used.

A slightly more complex structure was the object of test, consisting of a thin long Composite material beam with 4 piezoelectric components attached with a distance of 11 mm from the clamped extremity and 15 mm from its borders, as shown in Figure 7.

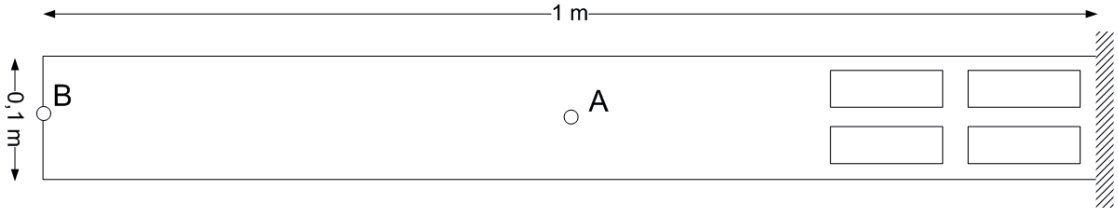

Figure 7: Simulation setup

Points A and B illustrated above are the points of interest in the displacement to be calculated. The nomenclature used for each one of the actuators is also important. Their position was chosen symmetrically so that their spacing should not affect the bending displacements. The material chosen for this test was the 914- carbon-epoxy tissue Composite Material with 2.4 mm of thickness. The ANSYS model is shown in Figure 8.

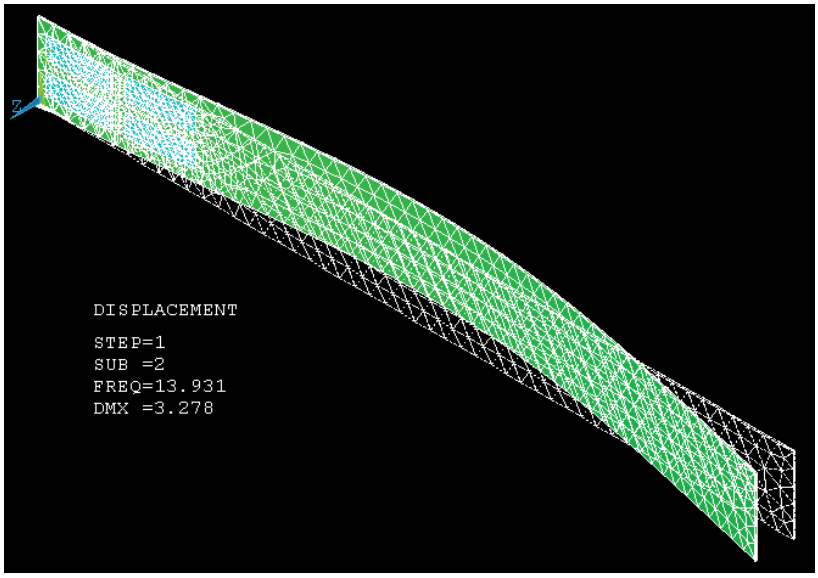

Figure 8 : Beam and MFC ANSYS model

It should be noted that the displacements indicated as outputs by ANSYS do not have physical sense. They are such that they displacement vector normalizes the mass-matrix to unity. The ANSYS simulation gives us the predicted proper frequencies, as well as the charges on the electrodes of the piezoelectric components; following the method proposed, these parameters are needed to calculate the numerical displacement at each of the studied points.

For the following analysis, the voltage values to be applied to each of the piezoelectric components are the same. This type of alimentation is used to generate bending movements of the structure. Since this comparison is being made only theoretically (with the use of the FEM software ANSYS), the quality factors are not known; a range of typical quality factor values will, therefore, be used in order to illustrate the tendency. Figure 9 shows the displacement values (at points A and points B) per unit of voltage to be applied to the piezoelectric components.

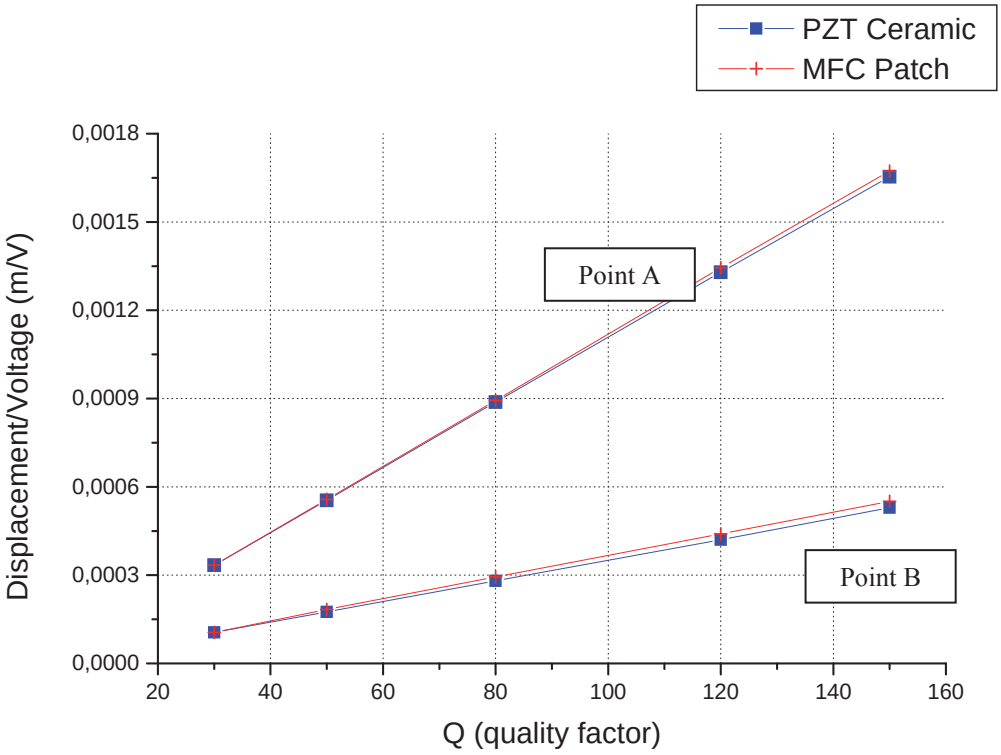

Figure 9 : Displacement/Voltage by Quality Factor for the 1st mode of vibration

Seeing as though the uncertainties of these results cannot be precisely calculated (the results come from FEM numerical solution, and therefore numerous factors come into play, such as meshing and element type choice), it cannot be concluded that the MFC Patch gives, for sure, better actuating capability than the PZT ceramic. It should be noted that the difference in absolute value of these parameters for each piezoelectric component is of the order of 10^{-6}, and therefore, for a voltage of the order of 10 V to 100 V, this difference will not surpass the order of 10^{-4}.

It can be concluded, all the while, that the substitution of the PZT ceramic by a MFC Patch does not, at least, compromise the active control system in terms of actuating capability efficiency. This conclusion validates a good reason for choosing microfiber composites as piezoelectric actuators, due to the previously mentioned advantages, among which can be cited its easy adaptability to complex geometry, simple repeatability in manufacturing, as well as its light-weighted durable, ready-to-use models.

6 CONCLUSION

With the help of ANSYS, a homogenized model of the Piezoelectric Macro Fiber Composite was elaborated and tested. A method for sizing piezoelectric actuators and sensors was studied and developed and put into practice with an experimental setup. The MFC model proposed, when in use with the sizing and positioning Modal Base Theory method presented, gave good results of displacement prediction for the first mode of vibration. The actuation/sensing capability of the MFC model was also put into comparison with that of the hard piezoelectric ceramics. The results were close enough to conclude that the MFC showed

to have an actuation capability as good as that of the ceramics. Along with this, the fact that it has a less brittle nature and is more easily adaptable to curved structures corroborates the statement that MFCs may replace the hard ceramics in Active Control systems.

A few aspects of the research still remain to be addressed by future projects in this topic. To better verify the proposed model, a closer analysis of the adhesive layer with Finite Elements modeling should be made. A study on how this layer behaves with the excitation of the structures' proper modes, for example, may help answer some of the questions that remained and were pointed out throughout the report.

The MFC patch model proposed was validated with the clamped beam experiment. The results for displacements at the first mode of vibration were very satisfactory, while the ones for the second mode were not as much. A future project could be concentrated into finding a way to validate the model experimentally with a more rigorous method. For this, a more accurate model of all components of the experiment should be well modeled; therefore this could be a consequence of the study of the adhesive layer behavior proposed in the topic above.

REFERENCES

SMART-MATERIAL©, *MFC Datasheet,* http://www.smart-material.com, Accessed September 14th, 2010.

IEEE; *Standards on Piezoelectricity* IEEE. 1988

A. DERAEMAEKER; S.BENELECHI; A. BENJEDDOU; A. PREUMONT; *Analytical and Numerical Computation of Homogenized Properties of MFCS: Application to a Composite Boom with MFC Actuators and Sensors*; *III ECCOMAS THEMATIC CONFERENCE ON SMART STRUCTURES AND MATERIALS*, 2007

V. POMMIER-BUDINGER; M.BUDINGER; J.RICHELOT; J.R. MARTINEZ; *Design of Structures with Piezoelectric Ceramics for Active Vibration Control*, Université de Toulouse, ISAE, 2008.

R. GALAN; *Étude des performances des actionneurs piézoélectriques pour le contrôle de vibrations sur des poutres en aluminium et en composite*. Projet de fin d'études, Institut Supérieur de l'Aéronautique et de l'Espace. Toulouse, 2008.